

# A Radio Polarimetric Study of the Galactic Center Threads

Cornelia C. Lang<sup>1,2</sup>, Mark Morris<sup>2</sup>, and Luis Echevarria<sup>3</sup>

## ABSTRACT

The Very Large Array has been used to carry out a multifrequency, polarimetric study of the non-thermal filaments (NTF's), G0.08+0.15, and G359.96+0.09, also known as the Northern and Southern Threads (Morris & Yusef-Zadeh 1985). These linear structures have been observed at  $\lambda=20, 6, 3.6$  and  $2$  cm, with high enough spatial resolution to be resolved for the first time at  $\lambda 6$  and  $\lambda 3.6$  cm. The  $\lambda 20$  cm image reveals a wealth of new detail in the radio sources lying within the inner 60 pc of the Galaxy. The Southern Thread has a prominent split along its length, similar to splitting at the ends of previously studied NTF's. In addition to the prominent Northern and Southern Threads, there are several elongated features that resemble NTF's, but extend for only 5–7 pc. With resolutions as fine as  $2''$ , the  $\lambda 3.6$  and  $\lambda 6$  cm images reveal a high degree of continuity and little substructure internal to the filament. However, the width of the Northern Thread varies along its length between  $\sim 4''$  and  $\sim 12''$  (0.15–0.5 pc), and becomes markedly diffuse at its NW extremity. The spectral index of the Northern Thread has been determined over a broad range of frequencies. Its flux density falls with frequency, ( $\alpha=-0.5$ ) between  $\lambda 90$  and  $\lambda 6$  cm (where  $S_\nu \propto \nu^\alpha$ ), and becomes much steeper ( $\alpha=-2.0$ ) between  $\lambda 6$  and  $\lambda 2$  cm. The spectral index does not vary significantly along the length of the Northern Thread, which implies either that the diffusion timescale for the emitting electrons is less than their synchrotron lifetime, or that the emitting electrons are reaccelerated continuously at multiple positions along the filament. Because of the lack of spectral index variation, we have not located the source of relativistic electrons. Polarization observations at  $\lambda 6$  and  $\lambda 3.6$  cm confirm the non-thermal nature of the emission from the Northern Thread. The fractional polarization in the Northern Thread reaches 70% in some regions, although the polarized emission is patchy. Large rotation measures ( $RM \gtrsim 2000$  rad m<sup>-2</sup>) have been observed with irregular variations across the filament; typical values of RM are 100–2000 rad m<sup>-2</sup>. The lack of any apparent pattern in the distribution of RM suggests that the Faraday rotating medium is not physically associated with the Northern Thread since the filament itself is so highly ordered. The intrinsic magnetic field in the Northern Thread is predominantly aligned along its long axis. The data on the Southern Thread were less conclusive: the Southern Thread was not detected in total intensity at  $\lambda 6$  or  $\lambda 3.6$  cm, while the polarized emission at  $\lambda 3.6$  cm arising from the Southern Thread is evident, with a bifurcated structure similar to that detected in total  $\lambda 20$  cm intensity.

---

<sup>1</sup>National Radio Astronomy Observatory, Box 0, Socorro, NM 87801; email: clang@nrao.edu

<sup>2</sup>Division of Astronomy, 8371 Math Sciences Building, Box 951562, University of California at Los Angeles, LA, CA 90095-1562

<sup>3</sup>Department of Physics & Astronomy, Arizona State University, Tempe, AZ

## 1. Introduction

In the past fifteen years, a number of unusual non-thermal filaments (hereafter, NTF's) have been observed with the Very Large Array (VLA)<sup>4</sup> in the inner regions of the Galaxy. These peculiar NTF's share the following characteristics (see reviews by Morris 1996; Morris & Serabyn 1996): (1) unique to the Galactic Center and found only within a projected distance of 150 pc from SgrA (assuming hereafter a distance of 8.0 kpc to the Galactic center; Reid et al. 1993), (2) lengths of tens of pc, yet widths of only  $< 0.5$  pc, (3) orientation essentially perpendicular to the Galactic plane within  $\sim 20^\circ$ , (4) strong linear polarization (up to  $\sim 50\%$ ), (5) spectral indices negative, flat or slowly rising, (6) rotation measures often  $> 1000$  rad  $m^{-2}$ , and (7) the intrinsic magnetic fields are aligned along the long axis of the filament. In addition, recent observations have found that each sufficiently well-studied NTF appears to be associated with the ionized edge of a molecular cloud.

The synchrotron nature of the radio emission from the NTF's was first proposed by Yusef-Zadeh, Morris, & Chance (1984), who discovered the NTF's in the Galactic center Radio Arc at  $\ell=0^\circ.2$ . Subsequent polarization studies of Tsuboi et al. (1986, 1995), Yusef-Zadeh & Morris (1987b), and Reich (1994) confirmed that the emission was strongly linearly polarized, and that the internal magnetic field orientations are parallel to the Radio Arc NTF's. The more isolated Northern and Southern Threads (G0.08+0.15 and G359.96+0.09) have been observed previously at  $\lambda=6, 20,$  and  $90$  cm with fairly low resolution (Morris & Yusef-Zadeh 1985; Anantharamaiah et al. 1991). These studies show that the spectral index of the Northern Thread between  $\lambda 90$  and  $\lambda 20$  cm is negative,  $\alpha = -0.6 \pm 0.1$ , and that the spectral index of the Southern Thread is nearly flat:  $\alpha = -0.04 \pm 0.03$ . Recent high resolution and polarimetric studies of the other NTF's, G359.1-0.2, the "Snake" (Gray et al. 1995) and G359.54+0.18 (Yusef-Zadeh et al. 1997), reveal fine sub-filamentation along the lengths of these NTF's and polarization properties similar to that of the Radio Arc NTF's. Observations at  $\lambda 20$  cm have also revealed a bifurcated NTF associated with the SgrC H II complex (Lizst & Spiker 1995).

There are a number of unresolved questions raised

by the unusual Galactic center NTF's. The most puzzling and fundamental of these is, what is the source of relativistic particles and the mechanism for their acceleration? The apparent associations between NTF's and both ionized and molecular gas provide a potential clue: is this association somehow related to, and necessary for, the generation of NTF's? Finally, what can the NTF's suggest about the overall magnetic field configuration at the Galactic center? and what can confine such narrow structures?

Several models of NTF generation have been proposed (see Morris 1996) and are summarized here. Benford (1988) and Morris & Yusef-Zadeh (1989) point out that the  $v \times B$  electric field induced at the surface of a molecular cloud moving at high velocity through a uniform magnetic field may be sufficient to accelerate electrons to relativistic energies. Heyvaerts et al. (1988) propose that the NTF's result from magnetic reconnection occurring at the interface of a magnetic loop expanding from the Galactic nucleus with a magnetic wall surrounding the central regions. Magnetic reconnection at the interface between adjacent magnetic pinches has also been invoked to explain electron acceleration in the bundle of NTF's which compose the Radio Arc (Lesch & Reich 1992). A recent model proposed by Rosner & Bodo (1996) suggests that the NTF's are formed as a result of the interaction of a fast, ionized stellar wind (emanating from a star with a high mass loss rate) with the ambient magnetic field. They argue that electrons could be accelerated to relativistic energies across the magnetopause, and loaded onto magnetic flux tubes, thus illuminating the NTF's. A more exotic idea proposed by Chudnovsky et al. (1986) is that the NTF's are manifestations of superconducting cosmic strings interacting with the magnetized plasma near the Galactic center.

Recent work on the NTF's has been aimed at determining the nature and the ubiquity of the interactions between the NTF's and the associated ionized and molecular gas. Based on high resolution CS(J=2-1) observations, Serabyn and Morris (1994; see also Serabyn & Güsten 1991) propose that the source of the electrons and their acceleration in the Radio Arc occurs at the intersection of these NTF's with the Sickle H II region and the underlying molecular cloud. Their observations showed that the molecular gas is distributed in clumps at locations where both the NTF's and ionized gas are present, and where changes in both brightness and continuity of

<sup>4</sup>The VLA is a facility of the National Science Foundation, operated under a cooperative agreement with the Associated Universities, Inc.

the Radio Arc NTF's occur (Yusef-Zadeh & Morris 1987c). Serabyn & Morris (1994) propose that at these positions, reconnection occurs between the magnetic field internal to the molecular cloud and the strong, external field, and may accelerate the electrons to relativistic energies, thus launching them to diffuse along the external field lines. These field lines are then illuminated by synchrotron radiation and thereby form an NTF. Morphological connections between the radio continuum, recombination line and molecular line observations in many NTF systems indicate that the model proposed by Serabyn & Morris (1994) may be widely applicable amongst the NTF's (e.g. Lizst & Spiker 1995, Uchida et al. 1996, Staguhn et al. 1998).

Here we present high resolution, multi-frequency data on the first isolated NTF's discovered, the Northern and Southern Threads, in order to test whether they share the properties as the other NTF's. Radio polarimetry has also been done in order to elucidate the synchrotron nature of these features, to determine their intrinsic magnetic field orientation, and to characterize the foreground Faraday screen.

## 2. Observations & Results

The multi-frequency observations presented here originate from several different epochs and configurations of the VLA. The frequency, phase center, and array information for all observations is summarized in Table 1. Standard AIPS procedures for calibration, editing, and imaging were used for all data. 3C 286 was used in all instances for flux calibration, and NRAO 530 (1733–130) and 1748–253 were used for phase and polarization calibration.

### 2.1. $\lambda 20$ cm Total Intensity Image

Figure 1 is a schematic diagram of the sources located in the inner 50 pc of the Galaxy, shown in Figure 2 and discussed throughout this paper. Figure 2 is the  $\lambda 20$  cm continuum image with a resolution of  $\sim 6''$ , made using the maximum entropy method of deconvolution, VTESS, in AIPS.

#### 2.1.1. *The Non-Thermal Filaments*

Both the Northern and Southern Threads are prominent features in Figure 2. The Northern Thread crosses the Arched Filaments (W1 and W2), and extends  $12'$  (30 pc) to the W from that point and  $3'$  (8 pc) to the E, with a total length of  $\sim 40$  pc. At the

E extremity of the Northern Thread,  $(\alpha, \delta)_{J2000} = 17\ 45\ 45, -28\ 51\ 30$ , there is another parallel filament of length  $\sim 4'$  (10 pc), but it is displaced  $20''$  to the S of the Northern Thread. It appears as if this second filament is a continuation of the Northern Thread. At  $\lambda 20$  cm, the Northern Thread exhibits very little variation in brightness or width and shows continuity along its length. It has, however, a gentle curvature, from where it is essentially parallel to the Radio Arc, to its W extremity, where it is oriented NW with a change of about  $20^\circ$  from its original orientation. At the W extremity, the Northern Thread appears bifurcated: a second faint filament runs parallel for  $\sim 2'$  (5 pc), and also becomes diffuse to the W.

The  $\lambda 20$  cm map provides new detail in the Southern Thread. This NTF extends for  $\sim 11'$  (28 pc), but is indistinct toward its E extremity, in the halo of the Sgr A complex. The Southern Thread has an average width of  $\sim 10''$  (0.4 pc) along its length, and shows a clear split toward its center, extending for  $\sim 4'$  (10 pc) along its length. The two parallel strands into which the Southern Thread is divided have about the same brightness, giving the impression of two filaments. Figure 3 shows a detail of the Southern Thread from the  $\lambda 20$  cm image shown in Figure 2. Although it is very faint, the more northern filament of the Southern Thread does appear to continue to at least the edge of the diffuse halo of the Sgr A complex. In addition, a possible third parallel filament is present just S of the split.

The NTF's of the Radio Arc also stand out in this image and show the sub-filamentation and fine structure which has been described by Yusef-Zadeh & Morris (1987b). However, in this image, the Radio Arc is at the edge of the primary beam here ( $30'$  at  $\lambda 20$  cm), and the NTF's are therefore not as well characterized as in previous images. Another feature in the  $\lambda 20$  cm image which resembles the NTF's is G359.79+0.17, located W of the Sgr A complex (Yusef-Zadeh 1986; Yusef-Zadeh & Morris 1987a; Anantharamaiah et al. 1991; Morris 1996); a detail of this filament is shown in Figure 4. At the diffuse, eastern edge of this filament, there appear to be multiple, parallel filaments, as described above for both the Northern and Southern Threads. This substructure has been confirmed by higher resolution, polarimetric observations, which also demonstrate that G359.79+0.17 shares all the characteristics of the NTF's (Lang & Anantharamaiah, in prep).

TABLE 1  
OBSERVED FIELDS

Field Designation	Array	Date	Frequency (GHz)	Phase center	
				$\alpha$ (J2000)	$\delta$ (J2000)
Sgr A Complex	CnB	27 June 1985	1.446	17 44 40.5	-28 51 14.0
	CnB	6 Oct 1986	"	"	"
	CnB	20 May 1989	"	"	"
	DnC	30 May 1987	"	"	"
	BnA	12 Feb 1987	"	"	"
Northern Thread 6	CnB	20 May 1989	4.585, 4.885	17 45 12.4	-28 46 46.6
	D	30 May 1987	4.585, 4.885	"	"
	BnA	28 Sept 1995	"	"	"
	DnC	22 Jan 1995	"	"	"
Northern Thread 3.6(a)	BnA	28 Sept 1995	8.085, 8.465	17 45 12.4	-28 46 46.6
	DnC	22 Jan 1995	"	"	"
Northern Thread 3.6(b)	BnA	28 Sept 1995	8.085, 8.465	17 43 30.4	-28 50 03.9
	DnC	22 Jan 1995	"	"	"
Northern Thread 2(a)	D	30 May 1987	14.460	17 45 12.3	-28 48 46.6
Northern Thread 2(b)	D	30 May 1987	"	17 45 19.1	-28 48 26.1
Northern Thread 2(c)	D	30 May 1987	"	17 45 27.9	-28 49 40.0
Southern Thread 6	BnA	28 Sept 1995	4.585, 4.885	17 45 09.8	-28 55 07.8
	DnC	22 Jan 1995	"	"	"
Southern Thread 3.6	BnA	28 Sept 1995	8.085, 8.465	17 45 09.8	-28 55 07.8
	DnC	22 Jan 1995	"	"	"

TABLE 2  
CENSUS OF LINEAR FEATURES PERPENDICULAR TO THE GALACTIC PLANE DETECTED IN FIGURE 2

Galactic Coordinates	Equatorial Coordinates		notes
	$\alpha$ (J2000)	$\delta$ (J2000)	
G0.16-0.15	17 46 00	-28 47 00	Radio Arc
G0.15-0.07	17 46 15	-28 51 30	'steep spectrum' filament S of Radio Arc
G0.08+0.15	17 45 15	-28 48 00	Northern Thread
G0.08+0.02	17 45 45	-28 51 30	extension of the Northern Thread
G359.96+0.09	17 46 05	-28 55 00	Southern Thread
G359.79+0.17	17 44 30	-29 02 00	curved filament
G359.98-0.11	17 46 00	-29 00 40	streak
G359.88-0.07	17 45 35	-20 04 00	streak
G0.02+0.04	17 45 30	-28 53 40	streak
G0.06+0.06	17 45 35	-28 51 40	quasi-linear features

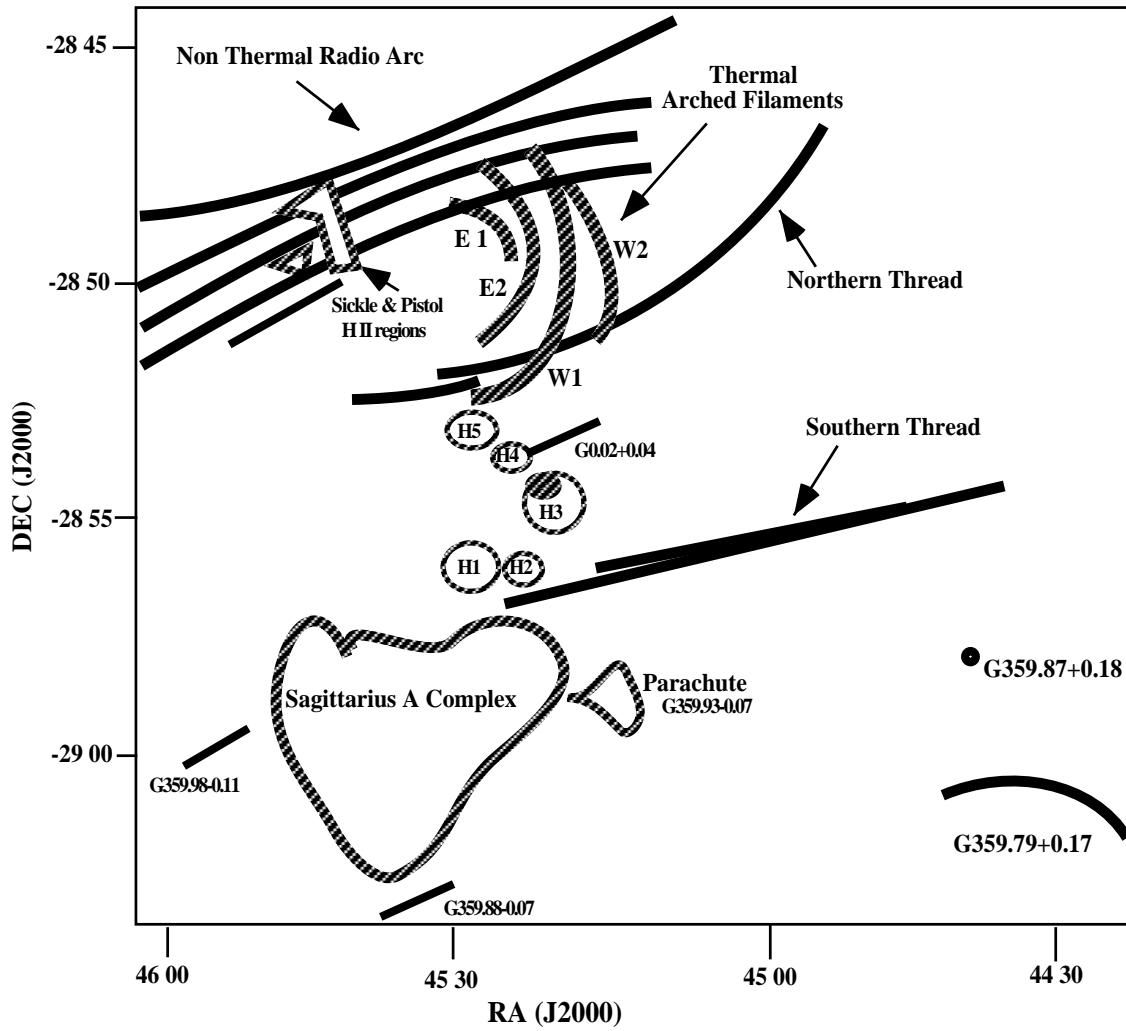


Fig. 1.— Schematic representation of the sources that are present in a 60 pc region of the Galactic center shown Figure 2 and discussed throughout this paper.

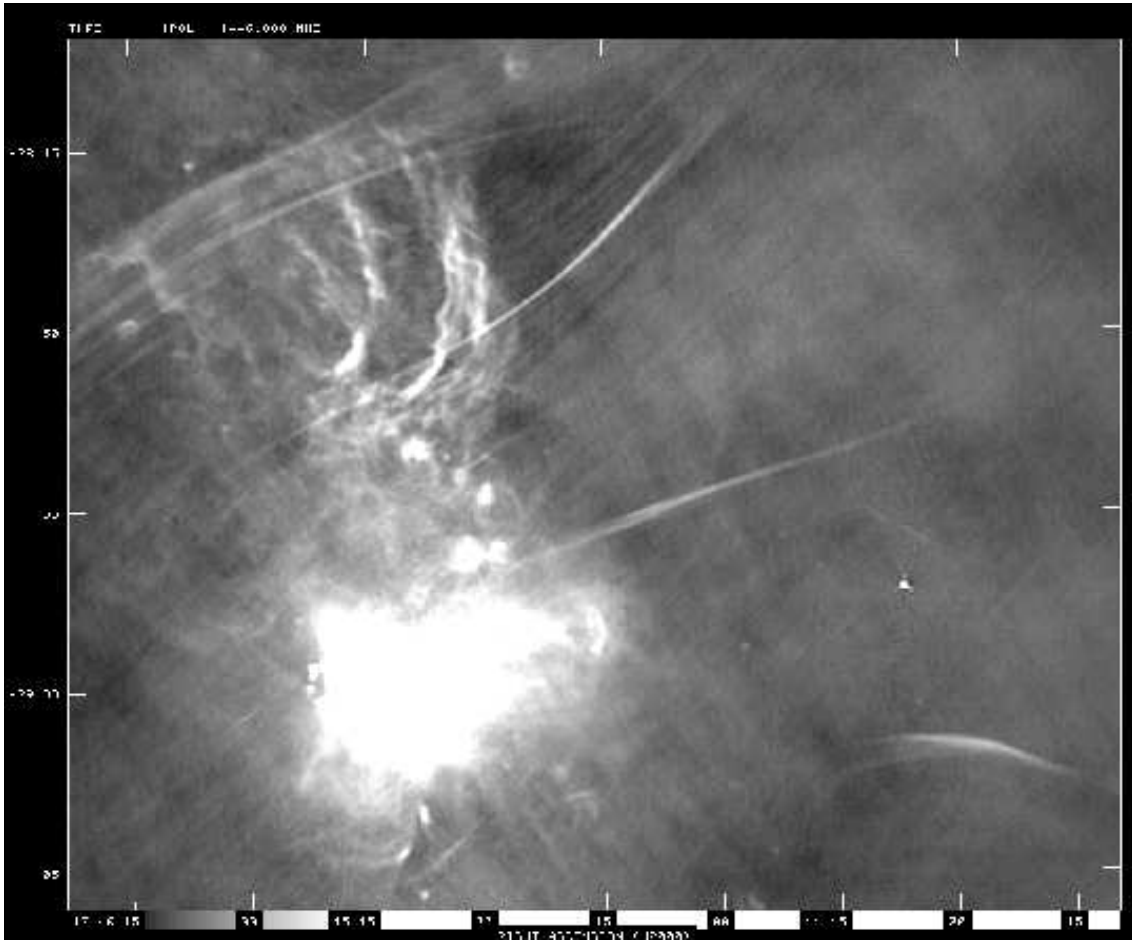


Fig. 2.—  $\lambda 20$  cm continuum image of a 60 pc region of the Galactic center, mostly at positive Galactic latitudes and longitudes. The resolution of this image is  $5''.90 \times 5''.5$ ,  $PA=80^\circ$ . The image was made with uniform weighing and has been corrected for the primary beam attenuation. The rms noise level in this image is  $0.5 \text{ mJy beam}^{-1}$ .

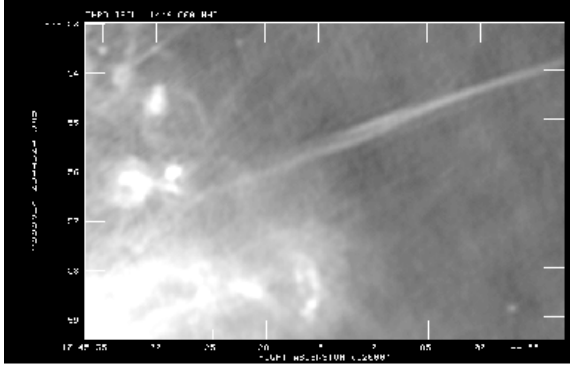


Fig. 3.— Detail of the Parachute, Southern Thread, and H sources (see Figure 1 for locations) from the  $\lambda 20$  cm image shown in Figure 2.



Fig. 4.— A detail from Figure 2 showing the filamentary source G359.79+0.17.

### 2.1.2. Additional Linear Structures: Streaks

Although the Threads are the most striking linear features in Figure 2, there are a number of other linear structures present which resemble the NTF's, although they only extend for 2–3' (5–7.5 pc). We refer to these features as “streaks”, following Yusef-Zadeh and Morris (1987a) who first identified several of them. A census of all filament-like sources detected in Figure 2, including streaks and known NTF's, is given in Table 2. Similar to the NTF's, the streaks are elongated perpendicular to the Galactic Plane and have comparable surface brightnesses. However, polarimetric observations are crucial for determining whether or not these streaks are the same class of objects as the NTF's. We note the following streaks in Figure 2 which are labelled in Figure 1: (1) G359.98-0.11, E of the SgrA complex; it is conceivable that this feature is a continuation of the NTF; (2) G359.88-0.07, S of the SgrA complex; (3) G0.02+0.04, S of the Arched Filaments, which appears to be associated with the H II region H4. Contour images of

two of these streaks are shown in Figures 5 and 6.

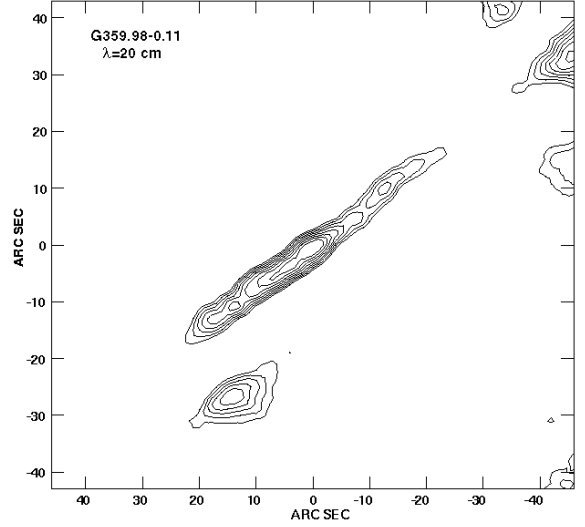


Fig. 5.—  $\lambda 20$  cm contour image of the elongated structure G359.98-0.11, classified as a “streak”. The contours in this image represent 2, 3, 4, 4.5, 5, 5.5, 6, 6.5, 7, 8, 9, 10, 11, 12, 13, 14  $\text{mJy beam}^{-1}$  levels, and the image is centered at  $(\alpha, \delta)_{2000} = 17\ 42\ 25, -29\ 03\ 28$ .

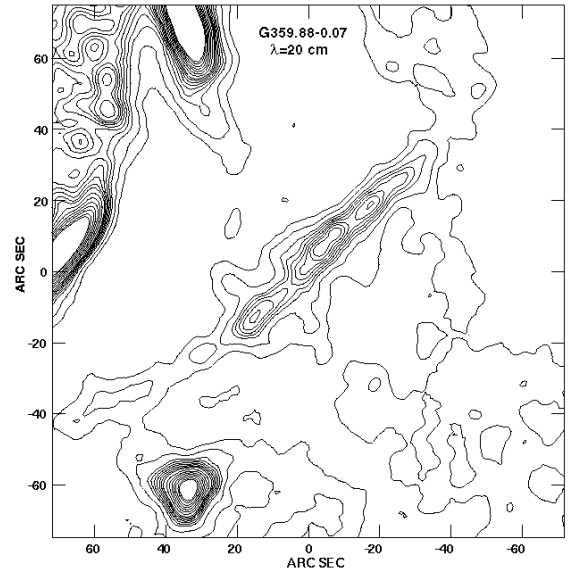


Fig. 6.—  $\lambda 20$  cm contour image of the streak, G359.88-0.07. The contours in this image represent 2.2, 2.4, 2.6, 3.0, 3.2, 3.4, 3.6  $\text{mJy beam}^{-1}$ , and the image is centered at  $(\alpha, \delta)_{J2000} = 17\ 42\ 50, -28\ 59\ 31$ .

TABLE 3  
SOURCES DETECTED NEAR THE GALACTIC CENTER IN THESE DATA

Galactic Coordinates	Equatorial Coordinates		notes
	$\alpha$ (J2000)	$\delta$ (J2000)	
G359.93-0.07	17 45 20	-28 58 20	"Parachute"; thermal source
G359.87+0.18	17 44 37	-28 57 09	FRII Galaxy (Lazio et al. 1999)
G0.09+0.17	17 45 08	-28 46 17	$S_{3.6}=1.0\pm 0.4$ mJy; $S_6=2.0\pm 0.6$ mJy

In addition to the streaks, a series of quasi-linear structures are apparent in Figure 2 within  $1'$  of  $(\alpha, \delta)_{J2000}=17\ 45\ 35, -28\ 51\ 40$ . These structures, first noted by Morris & Yusef-Zadeh (1989), are aligned perpendicular to the Galactic plane. Like the nearby Arched Filaments, these quasi-linear features may be thermally emitting structures, although the similarity of their orientation to the that of the nearby NTF's and streaks suggest that they have also been shaped by the magnetic field. Near the Radio Arc, we note an additional filament, previously reported by Anantharamaiah et al. (1991) and known as the 'steep spectrum filament'. This filament extends for  $3'5$ , running exactly parallel to and S of the Radio Arc NTF's. It may be associated with the Radio Arc, but as Anantharamaiah et al. (1991) point out, its spectral index is negative,  $\alpha=-0.4$ , compared to that of the Radio Arc:  $\alpha=+0.3$ .

### 2.1.3. Other Sources

The group of compact sources located between SgrA and the Arched Filaments are labelled in Figure 1 as H1–H5, after Yusef-Zadeh & Morris (1987a) and are known Galactic center H II regions. Several of these sources are highlighted in Figure 3. In particular, the H II region H3 shows a continuous ring-like structure. Radio recombination line studies reveal that these H II regions are likely associated with the  $-30$  km s $^{-1}$  molecular cloud (Serabyn & Güsten 1987), and can be characterized by  $T_e$ ,  $n_e$ , and  $\Delta_{VFWHM}$ , typical for Galactic center H II regions (Zhao et al. 1993). The source located at the W edge of the Sgr A complex (G359.93-0.07, or the "Parachute"), also evident in Figure 3 may be related to the "Streamers" which connect it morphologically

to SgrA (Yusef-Zadeh & Morris 1987a). Finally, the point source G359.87+0.18, detected earlier at  $\lambda 20$  and  $\lambda 90$  cm (Yusef-Zadeh & Morris 1987a; Anantharamaiah et al. 1991) is also apparent in Figure 2 at  $(\alpha, \delta)_{J2000}=17\ 44\ 37.2, -28\ 57\ 08$ . Lazio et al. (1999) have classified this source as a Faranoff-Riley II radio galaxy, based on VLA observations in the range of 0.33 to 15 GHz and an HI absorption spectrum. Table 3 summarizes the sources discussed in this section.

### 2.2. Total Intensity Images at $\lambda 6$ , $\lambda 3.6$ cm & $\lambda 2$ cm

Figure 7 shows the high resolution ( $\sim 2''$ )  $\lambda 6$  cm image of the Northern Thread and the Arched Filaments. At  $\lambda 6$  cm, the Northern Thread extends  $\sim 10'$  (25 pc), from its E extreme where it intersects the thermal Arched Filaments, to its W extreme where it becomes diffuse. We note a point source located near the W end of the Northern Thread (see Table 3). In previous observations (Morris & Yusef-Zadeh 1985; Anantharamaiah et al. 1991), the Northern Thread appears wider, due to lower resolution. However at  $\lambda 6$  cm, the Northern Thread is fully resolved for the first time. It is obvious in Figure 7 that the width of the Northern Thread changes along its length. Just E of the position where the Northern Thread crosses the Arched Filaments, it is narrowest,  $< 4''$  (0.15 pc). It becomes broader toward the W, with the largest width near its W extreme,  $\sim 12''$  (0.5 pc). The bifurcation of the W end of the Northern Thread detected at  $\lambda 20$  cm in Figure 2 is not observed at  $\lambda 6$  cm or  $\lambda 3.6$  cm. In addition, no apparent kinks or bendings occur along the Northern Thread, and there is no strong evidence for the type



of obvious sub-filamentation that has been observed in the Snake NTF (Gray et al. 1995), G359.54+0.18 (Yusef-Zadeh et al. 1997), and in the splitting of the Southern Thread.

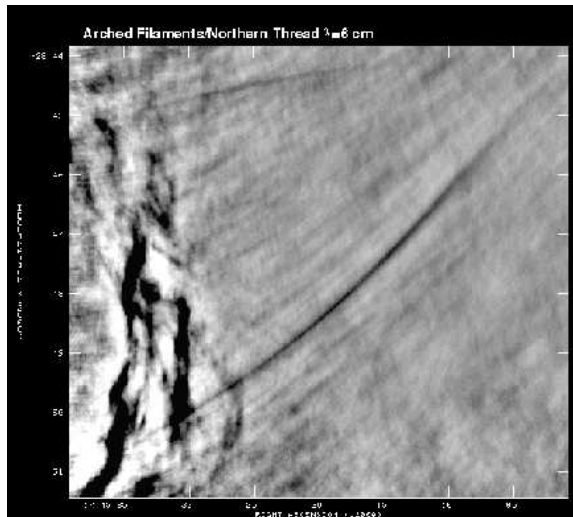


Fig. 7.— High resolution  $\lambda 6$  cm image shown in negative greyscale of the Northern Thread and a portion of the Arched Filaments H II regions. The image was made with uniform weighting and has a resolution of  $2''.12 \times 1''.73$ , PA= $0^\circ.91$ , and has been corrected for primary beam attenuation. The rms noise in this image is  $0.1 \text{ mJy beam}^{-1}$ .

Figure 8 shows a mosaic of the Northern Thread at  $\lambda 2$  cm, made from three overlapping fields. At such a high frequency, the Northern Thread can be followed for  $\sim 6'$  (15 pc) toward the W of the Arched Filaments. Total intensity images of the Southern Thread were also made at  $\lambda 6$  and  $\lambda 3.6$  cm, and in both cases, the Southern Thread does not stand out against the background of the SgrA complex. Upper limits for total  $\lambda 6$  and  $\lambda 3.6$  cm intensity are  $0.7 \text{ mJy beam}^{-1}$  and  $0.8 \text{ mJy beam}^{-1}$  respectively.

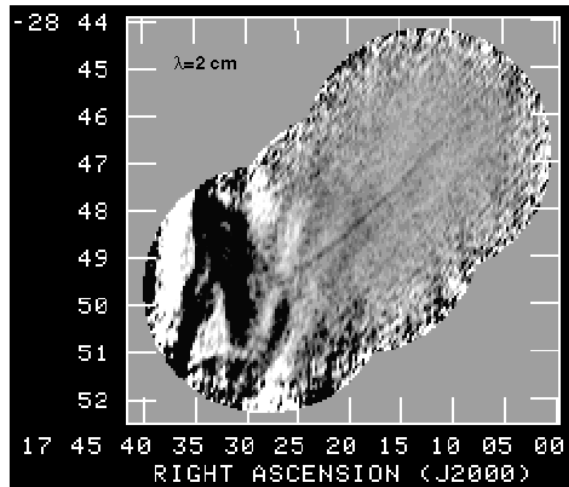


Fig. 8.—  $\lambda=2$  cm image of the Northern Thread and Arched Filaments shown in negative greyscale. This image is was mosaicked together from three fields, and has a resolution of  $4''.3 \times 4''.3$ .

### 2.2.1. Spectral Index of the Northern Thread

The surface brightness of the ridge of the Northern Thread at each of the four observed wavelengths is shown as a function of length along the NTF in Figure 9. From this figure, it is obvious that the surface brightness decreases with shorter wavelengths, and that  $\lambda 3.6$  and  $\lambda 2$  cm data do not cover the entire extent of the Northern Thread. Figure 10 shows the spectrum of the Northern Thread, sampled at different positions along its length. At 12 locations, the intensity was averaged over a narrow ( $8''$ ) region extending for  $40''$  perpendicular to the filament, in order to determine the local zero-level. After this baseline was subtracted, the flux density of the Northern Thread was measured at each position. The  $\lambda 90$  cm data were supplied by Anantharamaiah (priv. communication). Between  $\lambda 90$  and  $\lambda 6$  cm,  $\alpha \sim -0.5$ , and then a drastic steepening occurs between  $\lambda 6$  cm to  $\lambda 2$  cm, where  $\alpha \sim -2.0$ .

Caution must be exercised in comparing surface brightness between the different frequencies, since the the interferometer short spacings are less well sampled at the higher frequencies than at the lower frequencies, and we could be missing flux on the largest scales at  $\lambda 3.6$  and  $\lambda 2$  cm. However, our averaging procedure accounts for the different beam sizes and there is not strong evidence that significant flux has been resolved

out at higher frequencies, especially since the Arched Filaments, which have a larger angular extent, are clearly detected at all frequencies.

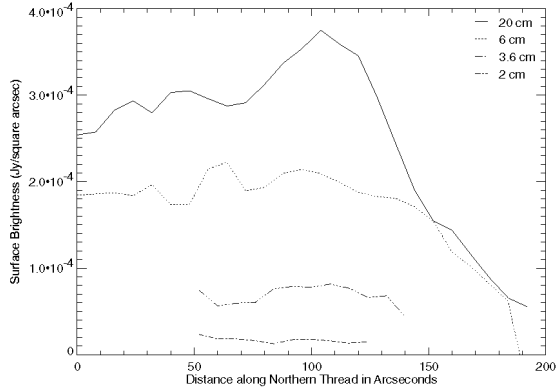


Fig. 9.— Surface brightness of the Northern Thread for each of the four observed frequencies as a function of length along the filament. The reference position for  $\lambda 6$  and  $\lambda 20$  cm is at  $(\alpha, \delta)_{J2000} = 17\ 45\ 20, -28\ 50\ 00$ , and increasing arcseconds westward from this position. At each frequency, the images have been adjusted to a common resolution ( $6''.2 \times 5''.5$ ), and the units are  $\text{Jy arcsecond}^{-2}$ .

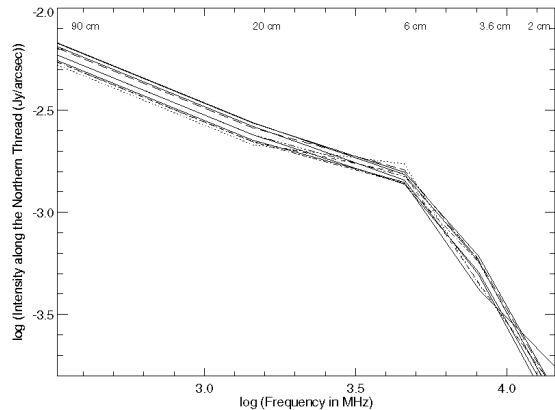


Fig. 10.— The spectrum of the Northern Thread: log-log plot of intensity per arcsecond along the Northern Thread as a function of frequency. The different linestyles correspond to different positions along the NTF at which the intensity was sampled. The sampling interval was  $8''$ , starting along the middle of the Northern Thread, and extending W for  $\sim 180''$ .

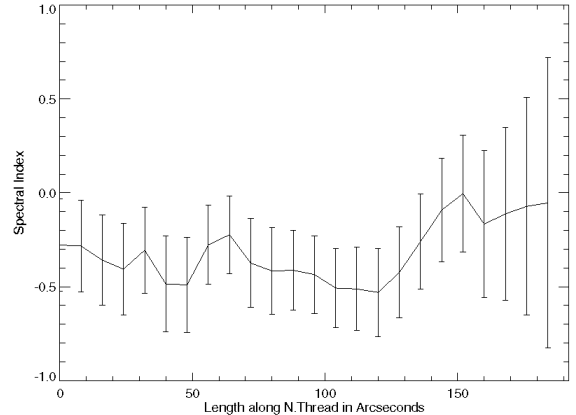


Fig. 11.—  $\lambda 20/6$  cm spectral index as a function of length along the Northern Thread, which is measured in arcseconds extending W from the position  $(\alpha, \delta)_{J2000} = 17\ 45\ 25, -28\ 50\ 00$ .

Figure 11 shows the  $\lambda 20/6$  cm spectral index as a function of length along the Northern Thread. Since the smaller primary beams of the  $\lambda 2$  and  $\lambda 3.6$  cm images do not include the entire extent of the filament (see Figure 9), a four-wavelength determination of the spectral index variation is not possible. Therefore, we determine the spectral index between  $\lambda 20$  and  $\lambda 6$  cm over an extent of  $180''$ , starting at  $(\alpha, \delta)_{J2000} = 17\ 45\ 25, -28\ 50\ 00$ , and look for variations westward from this position. Within the error bars, there is no significant variation of the spectral index along the length of the Northern Thread. Toward its diffuse W extent (between  $100$ – $180''$ ), we note a possible flattening in the spectral index.

### 3. Polarimetry Results

#### 3.1. Northern Thread

Stokes' Q and U images were made at  $\lambda 6$  cm (4.585 & 4.885 GHz) and  $\lambda 3.6$  cm (8.085 & 8.465 GHz), and images of the polarization angle ( $\text{PA} = \frac{1}{2} \text{Arctan}(\frac{U}{Q})$ ) and polarized intensity ( $I_p = \sqrt{Q^2 + U^2}$ ) were created. The observed polarization angles at  $\lambda 6$  and  $\lambda 3.6$  cm of the Northern Thread are shown in Figures 12 and 13.

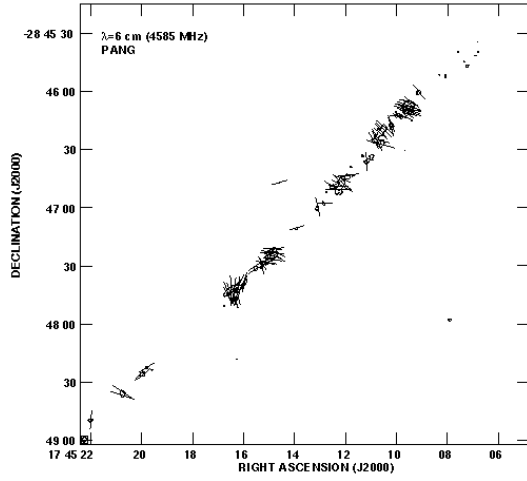


Fig. 12.— Observed polarization angle of the Northern Thread at  $\lambda 6$  cm. The contours represent polarized intensity, and the line segments are scaled in length to reflect the magnitude of the polarized intensity and show the orientation of the polarization angle of the detected electric vector ( $\theta=0^\circ$  is vertical and increases counterclockwise).

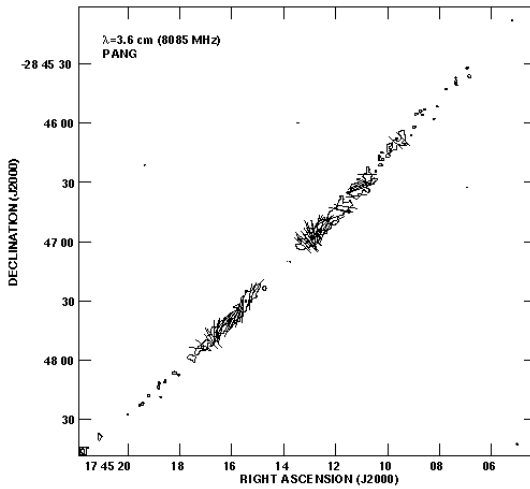


Fig. 13.— Observed polarization angle of the Northern Thread at  $\lambda 3.6$  cm, with contours and vectors in the same layout shown in Figure 12.

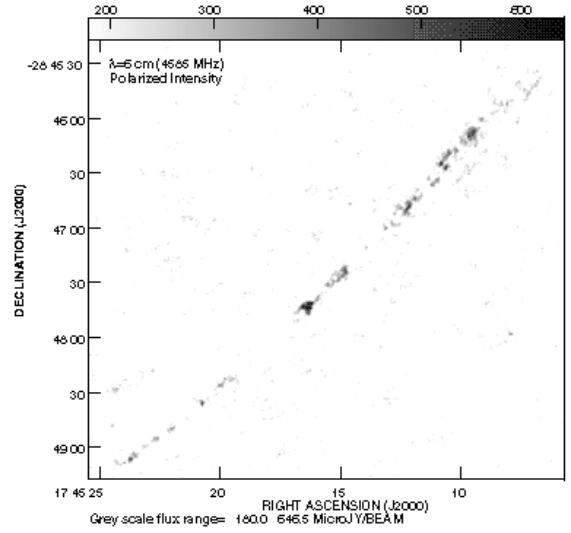


Fig. 14.— Polarized intensity at  $\lambda 6$  cm of the Northern Thread, shown in negative greyscale at a resolution of  $2''.5 \times 2''.0$ , PA= $0^\circ.5$ . The image has been blanked at the level of  $200 \mu\text{Jy}/\text{beam}$ .

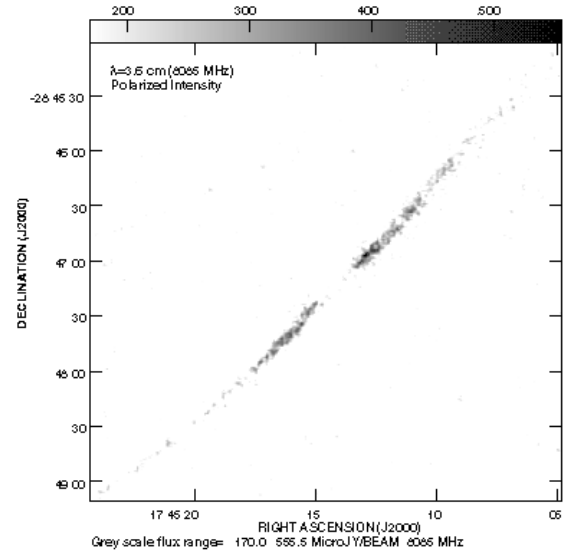


Fig. 15.— Polarized intensity at  $\lambda 3.6$  cm of the Northern Thread shown in negative greyscale at a resolution of  $2''.3 \times 1''.9$ , PA= $0^\circ.8$ . The image has been blanked at the level of  $170 \mu\text{Jy}/\text{beam}$ .

### 3.1.1. Distribution of Polarization

Figures 14 and 15 show the distribution of polarized intensity at  $\lambda 6$  cm and  $\lambda 3.6$  cm, respectively. In both cases, the polarized emission extends along the ridge of total intensity, but unlike the total intensity, its structure is patchy, and exhibits many gaps. At both  $\lambda 6$  and  $\lambda 3.6$  cm, polarized intensity is organized into clumps along the filaments, at a scale of  $\sim 5\text{--}10''$  ( $0.2\text{--}0.4$  pc). The peaks of polarized intensity, typically  $\sim 0.5$  mJy beam $^{-1}$ , define a very narrow ridge along the filament. The width of the distribution of polarized intensity appears to follow the pattern of total intensity; it becomes very narrow to the E and abruptly ends at  $(\alpha, \delta)_{J2000} = 17\ 45\ 25, -28\ 49\ 10$ , which corresponds to the position of the westernmost thermal Arched filament, intrinsically unpolarized in radio emission. A splitting into two parallel filaments of the  $\lambda 6$  cm polarized intensity at the W end of the Northern Thread is apparent in Figure 14. A similar splitting of the Northern Thread is detected in total  $\lambda 20$  cm intensity (Figure 2), however the positions of these splits do not exactly correspond. The polarized  $\lambda 6$  cm split occurs between  $\alpha_{J2000} = 17\ 45\ 00$  to  $17\ 45\ 10$ ,  $\delta = -28\ 46\ 30$ , whereas at  $\lambda 20$  cm the splitting is located at  $\alpha_{J2000} = 17\ 45\ 10$  to  $17\ 45\ 12$ ,  $\delta = -28\ 45\ 30$ . Curiously, this sub-structure is not detected in polarized emission at  $\lambda 3.6$  cm. The polarized emission at  $\lambda 3.6$  cm (Figure 15) is more coherent than that at  $\lambda 6$  cm and does not have such a patchy distribution. Similar patchy polarization structure has been observed in the Snake (Gray et al. 1995) and also in G359.54+0.18 (Yusef-Zadeh et al. 1997), and appears to be a common property of NTF's.

### 3.1.2. Fractional Polarization

The apparent fractional polarization as a function of length along the Northern Thread for both  $\lambda 6$  cm and  $\lambda 3.6$  cm is shown in Figure 16. The upper limit of fractional polarization for radio synchrotron emission under ideal conditions is 70% for  $\alpha = -0.5$  (Moffet 1975). Typical fractional polarization measures are determined to be in the range of 30–70% for the other NTF systems observed (Yusef-Zadeh & Morris 1988; Gray et al. 1995; Yusef-Zadeh et al. 1997). Here the maximum fractional polarization at  $\lambda 3.6$  cm is probably artificially high ( $>90\%$ ), owing to the fact that the largest scale structures of the total intensity are not fully sampled by the shortest spacings of the VLA, and therefore, a portion of the total flux den-

sity is missing. At  $\lambda 3.6$  cm, the largest angular scale to which the VLA is sensitive in the DnC array is on the order of  $100''$ , whereas the Northern Thread is  $\sim 10'$  in length. However, a qualitative trend is indicated in Figure 16: the fractional polarization at  $\lambda 3.6$  cm appears to increase from E to W along the Northern Thread. A more reliable calculation of fractional polarization could be obtained by combining single dish and interferometer total intensity data.

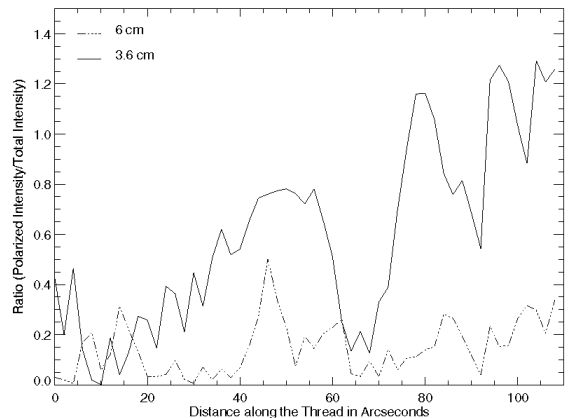


Fig. 16.— Fractional polarization at  $\lambda 3.6$  and  $\lambda 6$  cm as a function of length along the Northern Thread.

### 3.1.3. Rotation Measure

Using the four observed frequencies at  $\lambda 6$  cm (4.585 & 4.885 GHz) and at  $\lambda 3.6$  cm (8.085 & 8.465 GHz), the rotation angle as a function of wavelength was fitted to a  $\lambda^2$  law with the AIPS algorithm RM. The resultant distribution of rotation measure (RM) in the Northern Thread is shown in false-color in Figure 17. Figure 18 shows a sample fit of the polarization angle versus  $\lambda^2$  as a function of position for a small region of the Northern Thread, demonstrating that no ambiguities in the RM are present. The values for the RM toward the Northern Thread vary along the source from  $100$  rad  $m^{-2}$  to  $2300$  rad  $m^{-2}$ . Toward the center of the Northern Thread, the RM values are in the range of  $1000\text{--}2000$  rad  $m^{-2}$ . Along the NW extreme of the Northern Thread, where the total intensity becomes wider and more diffuse, the RMs have lower values,  $100\text{--}500$  rad  $m^{-2}$ .

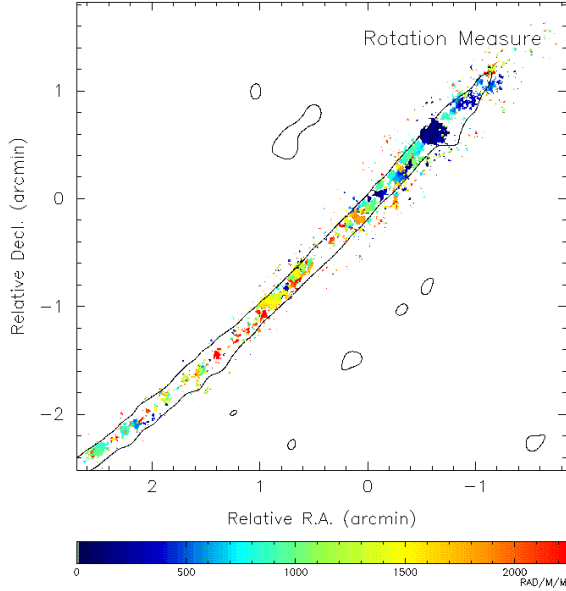


Fig. 17.— Distribution of rotation measure (RM) along the Northern Thread in false color scale with units of radians  $\text{m}^{-2}$ , with a resolution of  $2''.5 \times 2''.0$ . The superposed contour represents the  $3 \text{ mJy beam}^{-1}$  level of the  $\lambda 6 \text{ cm}$  total intensity image of the Northern Thread, which has been smoothed to a resolution of  $6''.2 \times 5''.5$ . The RM has been blanked for errors in the polarization angle that are greater than 10%.

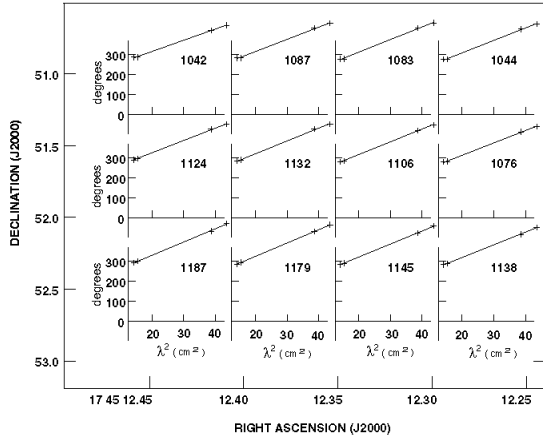


Fig. 18.— Fit to the polarization angle versus wavelength squared are shown as a function of position for a small region in the NW portion of the Northern Thread, where the rotation measures are low. The fits are plotted for every third pixel.

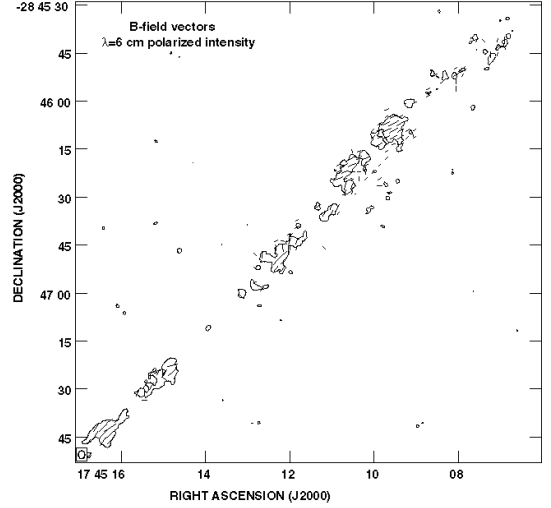


Fig. 19.— Vectors representing the intrinsic orientation of the magnetic field in the Northern Thread are shown superposed on the contours of polarized intensity at  $\lambda 6 \text{ cm}$ .

### 3.1.4. Intrinsic Magnetic Field

The vectors in Figure 19 represent the orientation of the magnetic field intrinsic to the Northern Thread obtained by correcting the observed position angles for Faraday rotation. The magnetic field is predominantly aligned parallel to the Northern Thread, as expected from the studies of other NTF's. In a few positions along the filament, there are deviations in the magnetic field orientation, up to  $45^\circ$  from alignment with the orientation of the NTF. Yusef-Zadeh et al. (1997) observe a similar effect in G359.54+0.18. They point out that such positions correspond to the edges of the “clumps” of polarization, where the RM gradient is also very high. In such places in the Northern Thread, the inferred direction of the magnetic field is not as reliable because the emission is nearly depolarized and the S/N is thus degraded.

## 3.2. Southern Thread

Although the Southern Thread is not detected in total intensity at this frequency, a low level of polarized intensity is detected. Figure 20 shows the distribution of polarization at  $\lambda 3.6 \text{ cm}$  of the Southern Thread. Using the upper limit for the total intensity at  $\lambda 3.6 \text{ cm}$ , we derive a limit for the fractional polarization in the Southern Thread

of  $\gtrsim 30\%$ . The splitting of the Southern Thread into two filaments is also apparent in the polarized intensity. For this filament, we did not attempt to derive the intrinsic magnetic field orientation since polarized emission is only detectable at two of the four observed frequencies. The polarization angle of the  $\lambda 3.6$  cm emission is shown in Figure 21.

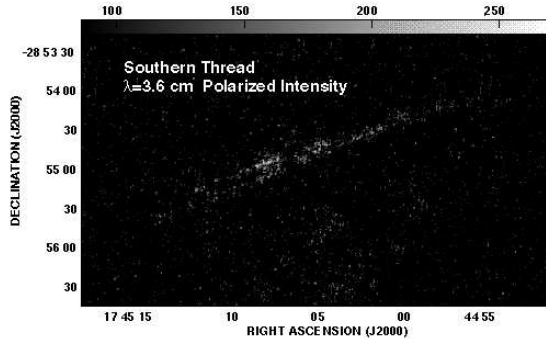


Fig. 20.— Polarized intensity at  $\lambda 3.6$  cm arising from the Southern Thread shown in greyscale, at a resolution of  $2''.0 \times 1''.5$ .

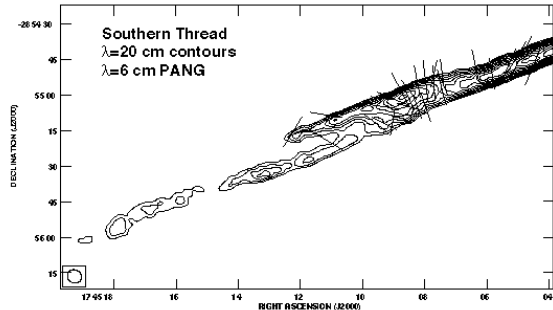


Fig. 21.— Observed polarization angle of the Southern Thread at  $\lambda 3.6$  cm, with vector orientation as in Figure 12.

## 4. DISCUSSION OF TOTAL INTENSITY RESULTS

### 4.1. Synchrotron Parameters

Using the formalism of Moffet (1975), we can derive an equipartition magnetic field strength from the radio continuum luminosity in the Northern Thread. Assuming that the filament is a cylinder, with length  $700''$  (30 pc) and radius  $6''$  (0.25 pc), we calculate an equipartition magnetic field strength of  $B_{eq} \sim 140 \mu\text{G}$ ,

comparable to the values derived for the NTF's in the Radio Arc using equipartition methods (Tsuboi et al. 1986; Yusef-Zadeh et al. 1987a; Reich 1994). The break in the spectrum at  $\nu_{cutoff} = 4.585$  GHz ( $\lambda 6$  cm) in Figure 10 implies a typical electron energy of  $\sim 1$  GeV, and a synchrotron lifetime of the electrons in the Northern Thread,  $\tau_{sync} \sim 4 \times 10^5$  years.

However, the magnetic field is unlikely to be in equipartition with the relativistic particles. If the particles are in equipartition with the magnetic field, then these filaments, which presumably trace the field, will be strongly distorted by interactions with the tumultuous medium in which they are embedded. The NTF's are observed to extend for up to 40 pc with no signs of local disturbances. Therefore, the highly organized field probably strongly dominates the energy density on the observed scales, in which case the magnetic field is substantially larger than the equipartition value, and the synchrotron lifetime correspondingly shorter. A more accurate estimate of the magnetic field strength in the Northern Thread may be obtained by equating the ram pressure or turbulent pressure of the molecular cloud that intersects the Northern Thread with the magnetic pressure of the NTF's (Morris & Yusef-Zadeh 1989). This argument rests on the fact that, in most cases, the NTF's appear rigid in their orientations at places where they are apparently interacting with the turbulent molecular gas. We deduce a lower limit of  $\sim 1$  mG for the Northern and Southern Threads has been estimated using this method (Morris & Yusef-Zadeh 1989), and similar arguments yielding similar field strengths have been applied to other NTF's.

### 4.2. Spectral Index Variation along the Northern Thread

According to the model of Serabyn & Morris (1994), the electrons which stream along the NTF in the Radio Arc are injected into the NTF's at the site of reconnection, where the ionized gas, molecular cloud and NTF's intersect. In the case of the Northern Thread complex, similar elements are present: (1) the magnetic Northern Thread, (2) the ionized Arched Filaments (Yusef-Zadeh 1986), which lie on the surface of (3) a molecular cloud with peculiar velocity of  $-30 \text{ km s}^{-1}$  (Serabyn & Güsten 1987). The site of acceleration would therefore be expected to lie at the intersection of the Arched Filaments and the Northern Thread. Thus, a steepening of the spectral index westward along the Northern Thread from

that point should be observed due to electron energy losses. However, as discussed in §2.2.1, no significant steepening of the spectral index westward along the length of the Northern Thread is detected.

A possible explanation for the lack of steepening is that the electrons may be diffusing along the filament more rapidly than they are losing energy via synchrotron radiation. To calculate the electron diffusion timescale, we assume that the Alfvén speed provides an upper limit on the speed at which the electrons diffuse along the filament (Alfvén 1942). The diffusion timescale has the following dependences on the electron density,  $n_e$ , and the magnetic field,  $B$ :  $\tau_{diff} \propto \frac{[n_e(\text{cm}^{-3})]^{1/2}}{B}$ . For  $n_e \lesssim 1 \text{ cm}^{-3}$ , and for a filament length of 30 pc,  $\tau_{diff} \lesssim 1.5 \times 10^4$  years ( $\frac{1}{B_{eq}}$ ). On the other hand, the synchrotron lifetime,  $\tau_{sync} = 1.7 \times 10^4$  years ( $\frac{1}{B} \frac{mG}{B_{eq}}$ )<sup>2</sup>. Since the timescales for synchrotron losses and diffusion are comparable, it is difficult to draw conclusions about the location of acceleration or reacceleration of the electrons along the filament, as a variation in the spectral index would be small, and not detectable within the current errors. A lack of variation of the spectral index is also observed along the Sgr C NTF (Kassim et al. 1999), and the Snake (Gray et al. 1995). The fact that the electrons are streaming along the NTF at a similar rate as they radiate their energy via synchrotron, raises the question: why do the NTF's terminate abruptly, fading quickly into the diffuse background?

### 4.3. Divergence of the Magnetic Field

One possible answer is that the divergence of the magnetic field, evidenced by the increase in width of the Northern Thread along its length, causes a reduction in the synchrotron emissivity. The observed intensity of synchrotron emission as a function of filament width,  $I(w)$ , can be modelled as arising from a cylindrical magnetic flux tube of width  $w$ ; this relation can be derived as follows.  $I(w)$  is proportional to the product of the synchrotron emissivity per particle,  $\epsilon$ , the number density of relativistic particles in the cylinder,  $n_e$ , and the depth of the cylinder, assumed equal to the width,  $w$ :  $I(w) \propto \epsilon \cdot n_e \cdot w$ . Further,  $\epsilon \propto B^{3/2}$ , where  $B$  is the magnetic flux density, and in turn, if the total magnetic flux within a filament is conserved,  $B \propto w^{-2}$ . Also, if the relativistic particle flux along an NTF is constant,  $n_e \propto w^{-2}$ .

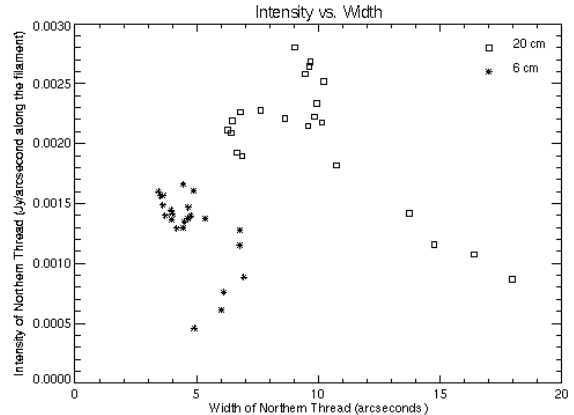


Fig. 22.— Plot showing intensity versus width of the Northern Thread for  $\lambda 6$  cm (stars) and  $\lambda 20$  cm (squares).

These relations imply that  $I(w) \propto w^{-4}$ . To assess the applicability of this scaling, we plot the  $\lambda 20$  cm and  $\lambda 6$  cm intensity of the Northern Thread as a function of its width in Figure 22. Although the data indicate that the intensity decreases with increasing width, more convincingly at  $\lambda 20$  cm than at  $\lambda 6$  cm, the slope of the decrease is not as steep as the predicted  $w^{-4}$ . One way to account for the weaker dependence is to note that the cross-section of a given flux tube may be elliptical rather than circular, and that the apparent change of width of the filament could correspond to variations in the orientation of the major axis of that ellipse (i.e., similar to a thick, twisting ribbon), rather than to a compression or divergence in the magnetic field. If the variation of intensity with width is due only to the change of orientation of the cross-section, then the magnetic field does not depend on the width, and the surface brightness depends only on the column density of relativistic particles, which goes roughly as  $w^{-1}$ .

Yet another possibility to explain the abrupt fading of the NTF's is that the decline of the ambient particle density with height above the plane, coupled with fewer sources of turbulence, (thus fewer density inhomogeneities), leads to a dramatic increase in drift velocity, and thus to the reduction of the density of relativistic synchrotron-emitting electrons.

### 4.4. Interaction with the Arched Filaments

The physical nature of the interaction between the Northern Thread, the Arched Filament H II regions, and the underlying molecular cloud in this region is

uncertain. Marked discontinuities in brightness of the Arched Filaments are apparent in Figure 23 where the Northern Thread intersects them. Figures 24 a & b show slices parallel to the Arched Filaments W1 and W2, over a distance of  $\sim 40''$  from N to S, roughly centered on the position where the Northern Thread intersects them. As evident in Figure 24a, the portion of W1 lying to the S of where the Northern Thread intersects it is dramatically brighter than the portion to the N of the NTF. In Figure 24b, there is a marked decrease in brightness of W2 S of the position where the Northern Thread intersects the thermal gas.

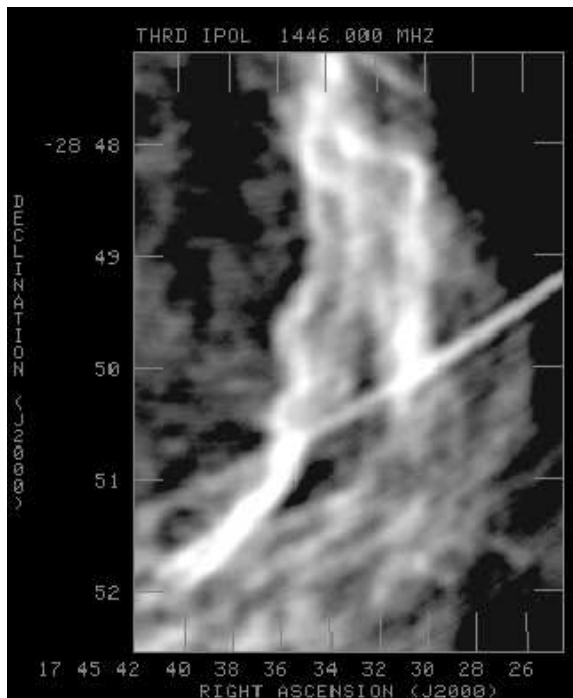


Fig. 23.— A detail from  $\lambda 20$  cm image in Figure 2, highlighting the positions where the Northern Thread intersects the Arched Filaments W1 and W2.

There is evidence in other NTF/ionized gas systems that the observed changes in brightness of intersecting sources imply a physical interaction between the sources. However, in the case of the Radio Arc NTF's, it is the brightness and continuity of the NTF's which change significantly at intersections with the Sickle H II region, rather than the thermal structures (Yusef-Zadeh & Morris 1987c). At this interface, magnetic reconnection has been suggested as the mechanism for acceleration of the electrons along the NTF's of the Radio Arc (Serabyn & Morris 1994),

but similar evidence for this mechanism in the case of the Arched Filaments and Northern Thread is not present.

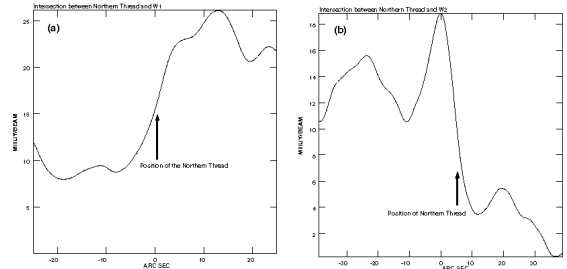


Fig. 24.— Slices in  $\lambda 20$  cm total intensity parallel to the Arched Filaments (a) W1 and (b) W2, over a distance of  $\sim 40''$  from N to S, at positions where the Northern Thread intersects the thermal gas.

#### 4.5. Motion of the Threads

The 3.9-year time base of the  $\lambda 20$  cm observations was used to put constraints on the transverse motion of the Northern and Southern Threads. The cosmic string model of Chudnovsky et al. (1986) predicts that NTF's should have relativistic, transverse motion. In order to detect possible transverse motion, we implemented the cross-calibration method proposed by Masson (1986). A difference image, made from differencing the data at two epochs, showed no evidence for transverse motion of the Northern and Southern Threads. We calculate upper limits of  $0.03c$  and  $0.06c$  for the lateral motion of any portion of the Northern and Southern Threads, respectively, thereby constraining relativistic lateral motion to the unlikely case of being entirely in or near the plane of the sky.

### 5. DISCUSSION OF POLARIMETRY RESULTS

#### 5.1. Sources of Depolarization

The observed polarization is extremely patchy, but similar small gaps in the polarization structure is observed in the other NTF's. In the case of the Radio Arc, the distribution of the polarized intensity has been attributed to depolarization by small-scale thermal media observed as large scale “helical” emission features apparently surrounding the Radio Arc (Yusef-Zadeh et al. 1984; Inoue et al. 1989). No thermal structures which could be causing the patchy depolarization are detected toward the North-



ern Thread, other than the Arched Filaments. The abrupt end of the polarized emission at the W extent of the Northern Thread can be attributed to the likelihood of the Arched Filaments lying at least partially front of the Northern Thread.

As apparent from Figures 14 and 15, the polarized emission at  $\lambda 3.6$  cm is more coherent and not as patchy as the  $\lambda 6$  cm polarized emission. This is consistent with a  $\lambda^2$ -dependence on rotation angle, which causes the beam depolarization to be larger at longer wavelengths. In addition, the overall high fractional polarizations and the large rotation of the plane of polarization ( $100$ – $300^\circ$ ; see Figure 18) indicate that the Faraday rotation is predominantly external to the filament. Internal Faraday rotation cannot rotate the plane of polarization by more than  $90^\circ$  without substantial depolarization (Burn 1966).

## 5.2. Faraday Rotation

In order to try to locate the Faraday rotating medium by associating it with either the source or with structures in the intervening medium, such as those detected by Inoue et al. (1989), we looked for coherent structures in the distribution of the rotation measure. None were detected. However, as described above, the large rotations are probably not due to internal Faraday rotation. Therefore, the Faraday screen is located near the distance of the NTF’s (i.e., at the Galactic center) or in a region somewhere along the line of sight. The highest values of RM observed in the Northern Thread ( $1000$ – $2500$  rad  $m^{-2}$ ) are similar to what has been observed toward other NTF’s. Gray et al. (1995) find RMs of  $2000$ – $5000$  rad  $m^{-2}$  along the Snake, with values increasing toward the Galactic plane. The RMs toward the linear filaments in the Radio Arc, located much closer to the plane than the Northern Thread, are  $2000$ – $5500$  rad  $m^{-2}$  (Yusef-Zadeh & Morris 1987b). Yusef-Zadeh et al. (1997) argue that the high RMs they observe in G359.54+0.18 (up to  $5000$  rad  $m^{-2}$ ) are more than two orders of magnitude larger than for sources outside of the inner Galaxy, and that the Faraday rotations are likely occurring closer to the Galactic center.

## 6. Ubiquity of the Magnetic Field in the Galactic Center

As discussed in Section §2.1.2, a number of linear structures similar to the known NTF’s are apparent in Figure 2. These “streaks” are aligned essentially

perpendicular to the Galactic plane, but extend for only  $5$ – $7$  pc, as opposed to the  $10$ ’s of pc extent of the NTF’s. The considerably shorter length might indicate that they are at a different stage in their development than the NTF’s. We note that the multiplicity of NTF’s and related linear features, such as streaks, may far surpass what we can observe with current sensitivity. The relatively uniform orientation of all of these features (perpendicular to the plane) is consistent with a simple, poloidal geometry for the magnetic field within the central few hundred parsecs of the Galaxy (Morris 1994). In fact, the multiple parallel filaments in both the Northern and Southern Threads (see Figs. 2 & 6) indicate that the synchrotron illumination of the magnetic field structure shifts to adjacent flux tubes along the length of the NTF’s, perhaps as a result of the lateral motion of the source of relativistic particles with respect to the ambient, pervasive field. Such a magnetic field can provide the support via magnetic pressure to account for the narrowly confined NTF’s, since magnetic pressure acts perpendicular to the field orientation. Models which rely on localized field enhancements (i.e. a local force-free field/current configuration) encounter difficulties providing a mechanism for keeping the NTF’s so highly collimated and with preventing their rapid expansion. In addition, the slight curvatures of the Northern Thread and the SgrC NTF are in opposite directions. This raises the possibility of a general divergence of the poloidal field at the Galactic center with increasing Galactic latitude. Indeed, allowing for projection effects, the large-scale curvature of all known NTF’s is consistent with such a divergence.

## 7. Conclusions

A multi-frequency study of the Northern and Southern Threads was carried out with the VLA using data from a number of different epochs and configurations. The following conclusions have been made:

(1) A  $\lambda 20$  cm image is presented of a  $60$  pc region of the inner Galaxy, mostly at positive latitudes and longitudes. The Sgr A West complex and the Northern and Southern Threads are prominent features. In addition, a number of new thermal and linear non-thermal sources are observed and discussed.

(2) The Southern Thread shows remarkable substructure at  $\lambda 20$ cm, but does not stand out against the diffuse halo of SgrA at  $\lambda 3.6$  cm and  $\lambda 6$  cm, except in  $\lambda 3.6$  cm polarized intensity.

(3) For the first time, the Northern Thread is resolved. In the total  $\lambda 6$  cm intensity image its width varies along its length, from  $\lesssim 4''$  (0.16 pc) at its narrowest position to  $\sim 12''$  (0.5 pc) at its most broadened position.

(4) The spectral index of the Northern Thread is relatively steep ( $\alpha = -0.5$  between  $\lambda 90$  and  $\lambda 6$  cm), with increasing steepness at the shorter wavelengths ( $\alpha = -2.0$  between  $\lambda 6$  and  $\lambda 2$  cm). The lack of significant variation of the spectral index along the filament prevents us from locating the source of acceleration of the emitting electrons.

(5) The polarized intensity arising from the Northern Thread is patchy and discontinuous along its length at  $\lambda 6$  cm, and is more coherent at  $\lambda 3.6$  cm. The fractional polarizations at  $\lambda 3.6$  cm are quite large in some places but likely to be upper limits because the total intensity on the largest scales may not be well sampled by the VLA.

(6) Values of the rotation measure range from 100–2300  $\text{rad m}^{-2}$  along the Northern Thread. The larger RM's are consistent with those observed toward NTF's. No coherent structures in the distribution of RM are observed which would give clues about the location of the Faraday rotating medium.

(7) The intrinsic magnetic field in the Northern Thread is primarily aligned with the filament.

(8) The Northern Thread shares all of the characteristics of the rest of the known NTF's: strong linear polarization, falling spectrum, large RM's in some locations, and an intrinsic magnetic field aligned along the filament length. Although the data were less conclusive on the Southern Thread, it, too, appears to show many of these characteristics. The large number of roughly aligned filamentary features in the  $\lambda 20$  cm image evokes the presence of a large-scale, dipole field permeating the inner 150 pc of the Galaxy.

We would like to thank G. Taylor of NRAO in Socorro for assistance with the polarization data, and M. Goss at NRAO in Socorro for assistance in imaging the  $\lambda 20$  cm data, and helpful comments on the manuscript. CCL acknowledges the RA Mentorship Fellowship at UCLA for support during the preparation of this manuscript.

## REFERENCES

- Anantharamaiah, K.R., Pedlar, A., Ekers, R.D., and Goss, W.M. 1991, MNRAS, 249, 262
- Anantharamaiah, K.R. 1997, priv. communication
- Benford, G. 1988, ApJ, 333, 735
- Burn, B. J. 1966, MNRAS, 133, 67
- Chudnovsky, E.M., Field, G.B., Spergel, D.N., Vilenkin, A. 1986, Phy Rev D, 34, 944
- Gray, A., Nicholls, J., Ekers, R.D., and Cram, L. 1995, ApJ, 448, 164
- Heyvaerts, J., Norman, C., & Pudritz, R.E. 1988, ApJ, 330, 718
- Kassim, N.E., LaRosa, T.N., Lazio, T.J.W., and Hyman, S.D. 1999, in the proceedings of the Tucson Galactic center workshop, *The Central Parsecs*, in press
- Inoue, M., Fomalont, E., Tsuboi, M., Yusef-Zadeh, F., Morris, M., Tabara, H., and Kato, T., 1989, in *The center of the Galaxy*, Morris, M., ed., IAU vol. 136, 269
- Lang, C.C. & Anantharamaiah, K.R., in prep.
- Lazio, T.J.W., Anantharamaiah, K. R., Kassim, N.E., & Cordes, J. 1999, ApJ, in press
- Lesch, H. & Reich, W. 1992, A&A, 264, 493
- Lizst, H., and Spiker, R. 1995, ApJS, 98, 259
- Masson, C. R. 1986, ApJ, 302, L27
- Moffet, A., 1975, in *Galaxies & the Universe*, vol. 10, Sandage, A. & M., and Kristian, J., ed., U of Chicago Press, 211
- Morris, M. 1994, in *The Nuclei of Normal Galaxies: Lessons from the Galactic center*, eds. R. Genzel, A. Harris, 185
- Morris, M. 1996, in *Unsolved Problems of the Milky Way*, Blitz, L. and Teuben, P., ed. Netherlands: IAU, vol. 169, 247
- Morris, M., and Yusef-Zadeh, F. 1985, AJ, 90 (12), 2511
- Morris, M., and Yusef-Zadeh, F. 1989, ApJ, 343, 703
- Morris, M., and Serabyn, E. 1996, A&A Review, 34, 645
- Reich, W. 1994, in *The Nuclei of Normal Galaxies* eds. R. Genzel, A. Harris, 55
- Reid, M. 1993, A&A Review, 31, 345
- Rosner, R., & Bodo, G. 1996, ApJ, 470, L49
- Serabyn, E., and Güsten, R. 1987, A&A, 184, 133
- Serabyn, E., and Güsten, R. 1991, A&A, 242, 376
- Serabyn, E., and Morris, M. 1994, ApJ, 424, L91
- Staghun, J., Stutzki, J., Uchida, K. I., Yusef-Zadeh, F., 1998, A&A, 336, 290
- Tsuboi, M., Inoue, M., Handa, T., Tabara, H., Kato, T., Sofue, Y., & Kaifu, N. 1986, AJ, 92 (4), 818
- Tsuboi, M., Kawabata, T., Kasuga, T., Handa, T., & Kato, T. 1995, PASJ, 47, 829
- Uchida, K.I., Morris, M., Serabyn, E., & Güsten, R. 1996, ApJ, 462, 768
- Yusef-Zadeh, F., Morris, M., & Chance, D. 1984, Nature, 310, 557
- Yusef-Zadeh, F., 1986, PhD Thesis, Columbia University
- Yusef-Zadeh, F. & Morris, M. 1988, ApJ, 329, 729
- Yusef-Zadeh, F. & Morris, M. 1987a, ApJ, 320, 545
- Yusef-Zadeh, F. & Morris, M. 1987b, ApJ, 322, 721
- Yusef-Zadeh, F. & Morris, M., 1987c, AJ, 94, 1178
- Yusef-Zadeh, F., Wardle, M., and Parastaran, P., 1997, ApJ, 475, L119
- Zhao, J.H., Desai, K., Goss, W.M., & Yusef-Zadeh, F. 1993, ApJ, 418, 235